Pharm Res (2012) 29:1328–1343
DOI 10.1007/s11095-011-0632-1

RESEARCH PAPER

Fe_3O_4-PEI-RITC Magnetic Nanoparticles with Imaging and Gene Transfer Capability: Development of a Tool for Neural Cell Transplantation Therapies

Humphrey H. P. Yiu • Mark R. Pickard • Cristina I. Olariu • Stephen R. Williams • Divya M. Chari • Matthew J. Rosseinsky

Received: 1 September 2011 / Accepted: 16 November 2011 / Published online: 2 December 2011

ABSTRACT

Purpose To develop Fe_3O_4-PEI-RITC magnetic nanoparticles with multimodal MRI-fluorescence imaging and transfection capability, for use in neural cell replacement therapies.

Methods The Fe_3O_4-PEI-RITC MNPs were synthesised through a multi-step chemical grafting procedure: (i) Silanisation of MNPs with 3-iodopropyltrimethoxysilane; (ii) PEI coupling with iodopropyl groups on the MNP surface; and (iii) RITC binding onto the PEI coating. The cell labelling and transfection capabilities of these particles were evaluated in astrocytes derived from primary cultures.

Results Fe_3O_4-PEI-RITC MNPs did not exert acute toxic effects in astrocytes (at ≤6 days). Cells showed rapid and extensive particle uptake with up to 100% cellular labelling observed by 24 h. MRI and microscopy studies demonstrate that the particles have potential for use in bimodal MR-fluorescence imaging. Additionally, the particles were capable of delivering plasmids encoding reporter protein (approximately 4 kb) to astrocytes, albeit with low efficiencies.

Conclusions Multifunctional Fe_3O_4-PEI-RITC MNPs were successfully prepared using a multi-step synthetic pathway, with the PEI and RITC chemically bound onto the MNP surface. Their combined MR-fluorescence imaging capabilities with additional potential for transfection applications can provide a powerful tool, after further development, for non-invasive cell tracking and gene transfer to neural transplant populations.

KEY WORDS astrocytes · cell transplantation · iron oxide nanoparticles · multifunctional nanoparticles · neural injury

ABBREVIATIONS

CHN	carbon, hydrogen, nitrogen
CNS	central nervous system
DAPI	4′,6-Diamidino-2-phenylindole
DLS	dynamic Light Scattering
FITC	fluorescein isothiocyanate
FTIR spectroscopy	Fourier transform infrared spectroscopy
GFAP	glial fibrillary acidic protein
GFP	green fluorescent protein
MCT	multiple comparison test
MNP	magnetic nanoparticle
MRI	magnetic resonance imaging
PBS	phosphate-buffered saline
PEI	polyethyleneimine
PVA	polyvinyl alcohol
RITC	rhodamine B isothiocyanate
RT	room temperature
TEM	transmission electron microscopy
TGA	thermogravimetric analysis
XRD	X-ray diffraction

H. H. P. Yiu
Chemical Engineering, School of Engineering and Physical Sciences
Heriot-Watt University
Edinburgh EH14 4AS, UK

M. R. Pickard · D. M. Chari (✉)
Institute for Science and Technology in Medicine, Keele University
Staffordshire ST5 5BG, UK
e-mail: d.chari@hfac.keele.ac.uk

C. I. Olariu · M. J. Rosseinsky (✉)
Department of Chemistry, University of Liverpool
Liverpool L69 7ZD, UK
e-mail: m.j.rosseinsky@liv.ac.uk

S. R. Williams
Imaging Science, Proteomics & Genomics Research Group
Manchester Academic Health Sciences Centre
University of Manchester
Oxford Road, Manchester M13 9PT, UK

INTRODUCTION

Neurological injury and disease of the central nervous system or CNS (*i.e.* the brain and spinal cord) inevitably has a poor clinical prognosis given its limited intrinsic regenerative capacity. Bypassing endogenous regenerative processes by transplantation of repair mediating cells constitutes a major strategy to promote repair (1). Several transplant populations have been identified (including genetically modified cell populations) that promote regeneration in experimental models of neurological injury and disease. Such research highlights a combination of four key technical aspects that must be considered, when evaluating neural cell transplantation therapies, in basic research and for translational applications.

The first is robust assessment of the safety of the transplant process with respect of both: (a) the transplant population (to avoid oncogenic effects, cell death and graft rejection); and (b) the surgical transplant procedures (with risks such as blood brain barrier breakdown, haemorrhage and embolism that can exacerbate the underlying pathology) (2).

The second critical, and often overlooked, consideration is the ability to identify/detect transplant populations *post* transplantation, using non-invasive imaging methods such as MRI, allowing for the examination of real time correlations between transplant cell survival/bio-distribution and functional neurological recovery. Several novel and clinical grade iron oxide nanoparticles (varying widely in size and composition) have been used to label neural transplant cells for such imaging applications (3).

Third, histopathological methods in post-mortem tissue are ultimately required for the detailed, micro-anatomical assessment of graft cell survival/integration in host tissue (4). Many methods have been used to label graft cells (*e.g.* carbocyanine dyes, bisbenzamides and reporter proteins). Alternative methods such as high dose x-irradiation of host tissue to deplete endogenous progenitor cells and remove the necessity for transplant cell pre-labelling, have also been adopted (5). Such methods can have major disadvantages such as toxicity, label diffusion and significant technical complexity.

The fourth consideration is achieving biomolecule delivery to transplant cells *ex vivo*, of particular relevance for 'combinatorial therapies' proposed in regenerative medicine (6). Such a strategy can further augment the regenerative properties of transplanted cell populations, for instance by exploiting the beneficial effects associated with their secretion of neurotrophic factors. Currently, this approach is heavily reliant on viral vectors (derived, for example, from retroviruses, lentiviruses and adenoviruses) which carry safety risks such as altered transplant cell proliferation/differentiation, toxicity and insertional mutagenesis, and have limitations for large scale production, restricting their experimental and clinical use. Many non-viral delivery methods (*e.g.* lipofection and electroporation) also have major drawbacks such as high cell loss and altered cell behaviour (7,8).

Clearly, a wide spectrum of methods is currently used to evaluate different aspects of neural cell transplantation and many have associated technical disadvantages. Critically, no single technique exists to achieve cell labelling as well as biomolecule delivery; therefore, two to three methodological steps are required to achieve these goals (for example, viral gene transfer for biomolecule delivery combined with cell labelling using a contrast agent/fluorescent dye). Such multi-step procedures involve extensive manipulation of cells prior to transplantation, which is undesirable from a safety perspective. Consequently, experimental studies in transplantation neurobiology inevitably focus on a single objective, such as imaging or biomolecule delivery. This has obvious limitations as all the above goals should be achieved to allow for the comprehensive evaluation/optimisation of a particular cell therapy. This lack of availability of multipurpose tools highlights an important need for the development of novel technologies, for a cohesive and integrative evaluation of neural cell transplantation therapies.

Nanotechnology platforms employing 'multimodal' iron oxide based magnetic nanoparticles (MNPs) could offer a novel solution to this technical challenge in transplantation neurobiology. MNPs have recently emerged as a fundamental tool for biomedical technology (9), due to advances in their large-scale synthesis (10) and complex surface functionalisation (11). These advanced nanomaterials are used in key areas of biomedicine, including drug/gene therapy (12), magnetic targeting (*e.g.* for cancer therapies) (13) and diagnostic imaging (as contrast enhancers) (14). The size and surface chemistry of MNPs can be adapted to suit the 'functionalising' molecule (15), consequently a tailored combination of surface functionalisation can be achieved to construct complex, multimodal particles that can mediate a variety of cellular applications whilst retaining nanoscale dimensions. To date, some magnetic particles have been tested for neural transplantation applications, such as graft labelling for MRI (16) and histological imaging (17), gene transfer for biomolecule delivery (7,8,18) and magnetic localisation of transplant cells (over areas of spinal cord injury) for minimally invasive cell delivery (19). However, few particles have been developed *specifically* for neural applications and no multifunctional MNPs have been described that can enable simultaneous gene transfer, cell targeting, cell labelling and MR imaging in neural cells. Further, the limited approaches described to date, to synthesise multifunctional MNPs use combined functionalities built

on a polymer backbone (such as chitosan) (20), decrease the iron content due to the thick, non-functional polymer coating and fail to exploit optimised nanoparticle chemistries to access high magnetisation (*M*) particles.

The goal of this study is to provide proof-of-concept of the chemical synthesis of a 'multimodal' MNP that is compatible for use in neural transplantation applications. We have employed a three-step chemical synthetic pathway to assemble a bi-functional surface on a MNP with fluorescent labelling and gene delivery ability, providing an adaptable platform for further modification and optimisation of the MNP functional surface. Unlike commercially available functionalised MNPs, the chemical grafting method adopted by us has avoided the use of crosslinked polymers on the shell, in order to minimise the overall particle size. The cell labelling and gene delivery potential of these 'prototype' MNPs was tested in astrocytes, a major candidate cell type for transplantation strategies to promote repair of neural injury.

MATERIALS AND METHODS

Materials

Iron (II, III) oxide (Fe_3O_4, magnetite) nanoparticles were purchased from Alfa Aesar, UK (Nanopowder, 20–30 nm (core size measured using TEM), 99%). 3-Propyliodotrimethoxysilane (95%) was purchased from Fluka. Polyethyleneimine (PEI, M_w=1,800, 50% aqueous solution), rhodamine B isothiocyanate (RITC) fluorescent dye, *N*,*N*-dimethylformamide (DMF, ACS Reagent grade) and chemicals for Perl's stain were purchased from Sigma Aldrich, UK. Sodium carbonate (99%) was purchased from Fisher, UK. DNA from calf thymus (activated, Sigma UK) was used for measuring the binding capacity of samples. Water was purified (deionised) with a Millipore system. Toluene (GPR grade, Fisher UK) was dried with activated molecular sieves (4 Å, Sigma Aldrich, UK) overnight prior to use. All other chemicals were used without further purification.

Cell culture reagents were purchased from Invitrogen (Paisley, UK) and Sigma (Poole, UK), and tissue culture-grade plastics were from Fisher Scientific, UK. The pmaxGFP plasmid, which encodes a green fluorescent protein (GFP) was from Amaxa Biosciences, Germany. Polyclonal rabbit anti-glial fibrillary acidic protein (GFAP) antibody was from DakoCytomation, UK, FITC-/Cy3-labelled secondary antibodies were from Jackson ImmunoResearch Laboratoratories Inc, USA and Vectashield mounting medium was from Vector Laboratories, UK. Neuromag (transfection-grade MNPs) and the Supermagnetic plate were purchased from Oz Biosciences, France. The care and use of all animals used in the production of cell cultures was in accordance with the Animals Scientific Procedures Act of 1986 (UK).

Synthesis of Fe_3O_4-PEI-RITC Magnetic Nanoparticles

A three-step functionalisation procedure was used to chemically bind PEI onto the surface of Fe_3O_4 nanoparticles, and then RITC was bound onto the PEI polymer skeleton (see Fig. 1a–c). In the first step, 0.5 g of unfunctionalised Fe_3O_4 nanoparticles was dispersed in dry toluene (50 ml) using an ultrasonic bath. 3-Iodopropyltrimethoxysilane (0.5 ml) was added to the Fe_3O_4 suspension and the reaction mixture was heated to 110°C with mechanical stirring. After 24 h, the solid was recovered using a rare earth NdFeB magnet and washed with acetone 5 times to remove residual toluene and silane. These functionalised nanoparticles, denoted as Fe_3O_4-I, were dried in a vacuum.

In the second step, Fe_3O_4-I nanoparticles (200 mg) were suspended in DMF (50 ml) with sonication. PEI (1.0 ml of a 50% aqueous solution) was added to the reaction mixture and heated to 130°C with mechanical stirring for 24 h. The nanoparticles were recovered using a NdFeB magnet and washed with acetone 5 times in order to remove residual DMF and PEI. Finally, the nanoparticles were dried in a vacuum. These nanoparticles are denoted as Fe_3O_4-PEI. For *in vitro* experiments, non-fluorescent Fe_3O_4-PEI nanoparticles, at 5 mg/ml concentration in deionised H_2O, were sterilised by heating at 100°C overnight.

Finally, in step 3, the free amine groups of Fe_3O_4-PEI nanoparticles were tagged with the fluorescent dye RITC, using a similar procedure to that normally employed for RITC coupling to protein molecules. Fe_3O_4-PEI (1 mg) was suspended in 1 ml of 0.5 M sodium carbonate buffer at pH 9.5 to ensure the deprotonation of amine groups on the PEI polymer coating. RITC solution (10 mg/ml DMSO; 0.08 ml) was then added to the Fe_3O_4-PEI suspension and the reaction mixture was covered with aluminum foil and rotated using a Stuart SB2 Rotator at room temperature overnight. The RITC-tagged Fe_3O_4-PEI was finally washed with deionised H_2O until no further fluorescence was observed in the supernatant. The sample is denoted as Fe_3O_4-PEI-RITC.

Characterisation of Fe_3O_4-PEI-RITC MNPs

Fourier Transform Infrared Spectrometry (FTIR) spectra were obtained from powder samples on a Perkin-Elmer Universal ATR spectrometer. For each sample, 20 scans in the region from 650 to 4,000 cm^{-1} were accumulated with a resolution of 4 cm^{-1}. XRD was carried out on a PANalytical Xpert system using Co $K\alpha_1$ radiation. Scherrer analysis was carried out using the Xpert Highscore Plus software. CHN elemental analysis was

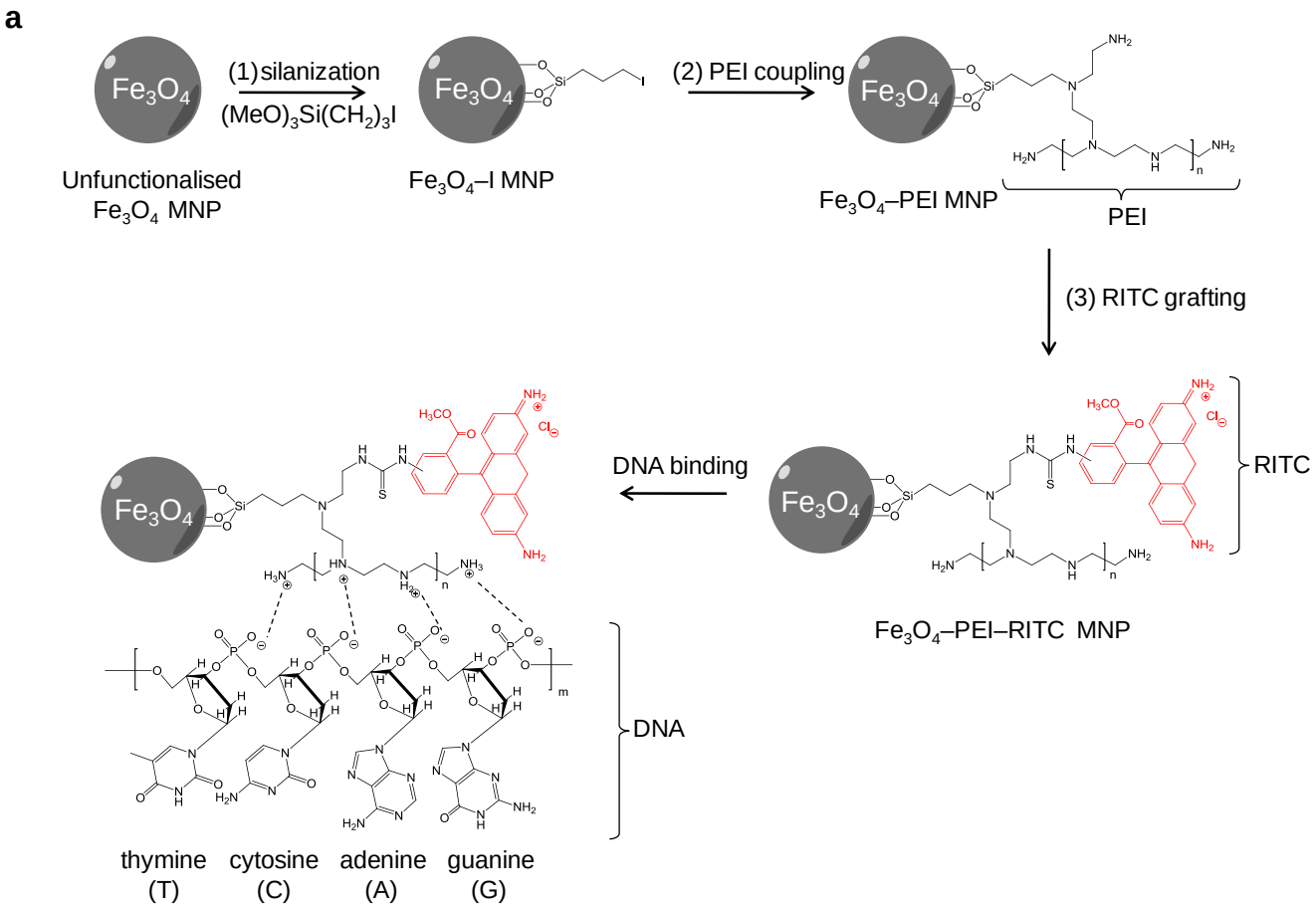
a
Fe3O4
(1) silanization
(MeO)3Si(CH2)3I
Fe3O4
(2) PEI coupling
Fe3O4
Unfunctionalised
Fe3O4 MNP
Fe3O4–I MNP
Fe3O4–PEI MNP
PEI
(3) RITC grafting
DNA binding
RITC
Fe3O4–PEI–RITC MNP
DNA
thymine
(T)
cytosine
(C)
adenine
(A)
guanine
(G)

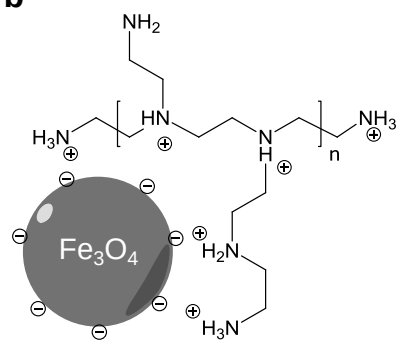
b
Fe3O4

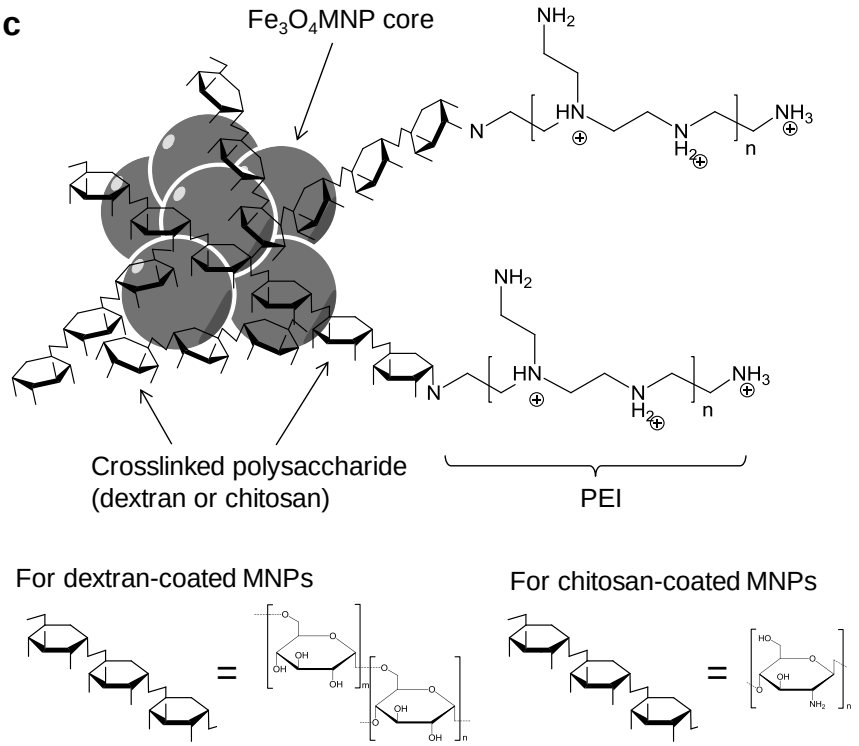
c
Fe3O4MNP core
Crosslinked polysaccharide
(dextran or chitosan)
PEI
For dextran-coated MNPs
For chitosan-coated MNPs

◀ **Fig. 1** Schematic diagrams of particle synthesis and basic design. (**a**) The three step chemical synthetic pathway of Fe_3O_4-PEI-RITC magnetic nanoparticles. Step 1 (silanisation) is to graft the MNP surface with iodopropyl groups using 3-iodopropyltrimethoxysilane. Step 2 involves a coupling reaction between amine groups on the PEI polymer and the iodopropyl groups on the surface of Fe_3O_4-I MNPs. Step 3 involves RITC binding onto the PEI coating. The DNA binding occurs as the grafted PEI possesses positive charges. (**b** and **c**) Schematic diagrams showing the basic design of PEI-coated MNPs commonly found in the literature. (**b**) PEI-coated MNPs using passive (or electrostatic) coating method. (**c**) Crosslinked polysaccharide-coated MNPs grafted with PEI using binding agents such as glutaraldehyde. Figures are drawn not to scale and the crosslinked polysaccharide structures in (**c**) are only for illustrative purposes, not to present the exact chemical structure of these coatings and the PEI coupling chemistry.

carried out to analyse the organic content of the functionalised samples, using a Thermo Flash EA1112 Series analyser, because the organic content directly influences the overall iron content of the MNPs (for comparison, commercial functionalised MNPs usually have an organic content of 80–90%) (21). The morphology of functionalised Fe_3O_4 nanoparticles was studied using a transmission electron microscope (TEM, Tecnai G2 Spirit BioTWIN) at 100 keV. The zeta potential of the particles in unbuffered deionised water was recorded using a Malvern Zetasizer Nano ZS.

To quantify the DNA binding capacity of samples, nanoparticles (10 to 75 μg) were mixed with 100 μg of DNA in 1.0 ml deionised water. The suspensions were incubated at room temperature under rotation. After two centrifugations, the unbound DNA in the supernatant was determined by UV–vis spectrophotometry at 260 nm. The amount of DNA bound onto the particles was calculated by subtracting the unbound DNA concentration from the total DNA concentration (determined by UV–vis spectrophotometry of DNA solution with no particles added). Each binding experiment was repeated 3 times and average values of the three experiments were plotted as the DNA binding curve.

MRI images of Fe_3O_4-PEI-RITC MNPs at various Fe concentrations (0.01 mM, 0.05 mM, 0.1 mM, and 0.2 mM) were acquired using a Bruker Avance III console and gradient system interfaced to a Magnex Scientific 7T, horizontal bore magnet at a 1H resonant frequency of 300 MHz. T_2 was calculated from a set of RARE (22) images acquired with TR = 10,000 ms and TE values of 11, 33, 55 and 77 ms.

Evaluation of MNP Labelling and Transfection in Astrocyte Cultures

Preparation of Astrocyte Cell Cultures

Mixed glial cultures were established from cerebral cortices of neonatal Sprague–Dawley rats, and astrocytes were purified from these by sequential mechanical shaking, using a published procedure (18). The adherent astrocyte cell layer was trypsinized, and either subcultured once in poly-D-lysine (PDL)-coated T-75 flasks or used directly to seed PDL-coated 8-well chamber slides (cell density of 0.25×10^5 cells/cm^2) for experiments to assess culture purity, Fe_3O_4-PEI-RITC uptake and related cytotoxicity, and particle-mediated transfection of a reporter gene. Culture medium used throughout was D-10 medium (Dulbecco's modified Eagle's medium supplemented with 2 mM glutaMAX-I, 1 mM sodium pyruvate, 50 U/ml penicillin, 50 μg/ml streptomycin and 10% fetal bovine serum), and all cultures were incubated at 37°C in 5% CO_2/95% air, with medium changes every 2–3 days.

MNP Uptake, Transfection and Cytotoxicity Experiments

The potential of the Fe_3O_4-PEI-RITC particles for both cell labelling and gene delivery applications was assessed. For the latter application, this necessitated the formation of particle-DNA complexes prior to adding to cells. The physiochemical properties of nanoparticles, notably size and surface charge, can markedly influence their uptake by cells, and consequently cytotoxicity. Since the size and charge of unmodified Fe_3O_4-PEI-RITC particles is likely to be different from particle-DNA complexes, particle uptake and related cytotoxicity experiments were conducted by incubating cells with (i) unmodified Fe_3O_4-PEI-RITC particles alone; and (ii) Fe_3O_4-PEI-RITC particle-DNA complexes in adjacent wells of each astrocyte culture. The DNA used for these experiments comprised a plasmid, pmaxGFP, which encodes green fluorescent protein (GFP), to facilitate evaluation of the gene delivery potential of particles, and the transfection protocols employed were based on a published procedure (18).

At 24 h after cell seeding, medium was replaced with fresh D-10 medium (0.15 ml), and cells were cultured for at least 1 h before addition of particles alone, DNA alone or transfection complexes. To prepare transfection complexes, pmaxGFP plasmid was diluted in 18 μl DMEM base medium (without supplements), then added to 12 μl Fe_3O_4-PEI-RITC and gently mixed by pipetting; the following total amounts of pmaxGFP plasmid and Fe_3O_4-PEI-RITC were studied: (i) 800 ng and 12 μg, respectively; (ii) 267 ng and 4 μg, respectively; (iii) 89 ng and 1.3 μg, respectively; and (iv) 800 ng and 0 μg, respectively (DNA only control well). Particles alone were prepared in parallel in a similar manner but contained deionised water instead of DNA. After 20 min, the entire mix (30 μl) of complexes or particles alone was added dropwise to cells, whilst gently agitating the chamber slide. Medium was usually replaced with D-10 medium alone (no particles or DNA) at 24 h *post*-particle addition. In experiments to determine the

long-term intracellular retention and disposition of particles, this medium change was performed at 4 h. Living cells were regularly monitored by phase contrast/fluorescence microscopy for up to 144 h *post*-particle application for evaluation of particle uptake/retention, GFP expression and particle-associated cytotoxicity (effects on cell adherence, cell morphology and culture growth). For quantification of MNP uptake, samples were fixed in 4% paraformaldehyde at 24 h for assessment of particle uptake and cytotoxicity, and at 48 h for assessment of transfection efficiency.

Magnetofection Experiments (Static Field Application)

Additional experiments to assess the effect of a static magnetic field on transfection efficiency (magnetofection) were conducted in a similar manner, except slides containing particle-DNA complexes only (or DNA only for controls) were placed on the Supermagnetic plate for the first 30 min after the addition of complexes to cells. In some transfection experiments, Fe_3O_4-PEI particles were substituted for Fe_3O_4-PEI-RITC particles, to exclude effects of the RITC tag on the gene delivery capacity of the particles. In addition, to verify plasmid quality and the transfection competence of cultures, Neuromag-mediated transfection (± static magnetic field) of astrocyte cultures with pmaxGFP was tested according to a published procedure (18), modified (as above) for use with 8-well chamber slides; final concentrations of Neuromag and pmaxGFP were 0.7 µl/ml and 0.2 µg/ml, respectively.

Immunocytochemistry and Histochemistry

Cells were washed three times with phosphate-buffered saline (PBS) then fixed with 4% (w/v) paraformaldehyde (in PBS) for 20 min. Samples were then again washed three times with PBS. For immunocytochemistry, fixed samples were incubated with blocking solution (5% normal donkey serum in PBS-0.3% Triton X-100) (room temperature, RT, 30 min), then with the GFAP antibody (1:500 in blocking solution; 4°C, overnight) for identification of astrocytes. After washing, samples were incubated with blocking solution (RT, 30 min), then with either FITC- or Cy3-labelled donkey anti-rabbit IgG (1:200 in blocking solution; RT for 2 h) for uptake and transfection experiments respectively. Samples were then washed and mounted with Vectashield mounting medium containing 4′,6-diamidino-2-phenylindole (DAPI) to visualise nuclei. For Perl's Prussian Blue staining to visualise intracellular iron, fixed cells were incubated with 2% potassium ferricyanide in 2% HCl for 30 min, washed three times with distilled water and mounted with Vectashield mounting medium without DAPI.

Fluorescence Microscopy and Image analysis- Quantification of MNP Uptake

Live cells were imaged using an inverted fluorescence microscope equipped with phase-contrast optics (Leica DM IL LED inverted microscope). Fluorescence microscopy of mounted slides was performed using an Axio Scope A1 microscope (Carl Zeiss MicroImaging GmbH, Goettingen, Germany); images were captured at fixed exposure settings then merged using image analysis software. To calculate culture purity, DAPI-stained nuclei were scored for association with GFAP. To calculate the proportions of astrocytes demonstrating particle uptake (termed % labelled cells), GFAP-positive cells were scored for the presence of Fe_3O_4-PEI-RITC. To calculate the proportions of GFP-expressing cells (termed transfection efficiency), nuclei were scored for association with GFP.

To assess cytotoxicity of particles alone or after complexing with plasmid, DAPI stained nuclei of GFAP-positive cells were assessed visually for pyknotic changes (nuclear shrinkage, fragmentation, DNA condensation) and cells were additionally assessed for aberrant GFAP staining (*i.e.* intensity/cellular distribution of stain). For all quantifications, a minimum of 100 GFAP-positive cells per treatment were evaluated. In addition, to assess the adherence of astrocytes post particle addition, the number of GFAP-positive cells per microscopic field was determined; a minimum of 3 microscopic fields (X200 magnification) were assessed.

Statistical Analysis

Data are expressed as mean ± SEM. To assess the effects of MNP concentration on the proportion of cells showing particle uptake, data were analysed by a one-way ANOVA followed by Bonferroni's post-tests. One-way ANOVA with Dunnett's multiple comparison test (MCT) was used to analyse cytotoxicity data.

RESULTS

Characterisation of Fe_3O_4-PEI-RITC MNPs

The nature of the grafted PEI coating on Fe_3O_4-PEI-RITC MNPs was characterised using FTIR spectroscopy (Fig. 2a). The characteristic peaks of PEI (NH_2 vibration from 3,300 to 3,200 cm^{-1}, CH_2 stretching at 2,910 cm^{-1} and CH_2 bending at 1,460 cm^{-1}) were observed due to the chemical structure of the PEI polymer coating on the MNPs. The XRD pattern in Fig. 2b also confirms the inverse spinel crystal structure of the core Fe_3O_4. Using CHN elemental analysis, the amount of PEI grafted onto the surface was found to be 0.11 mmol/g or 117 PEI molecules per

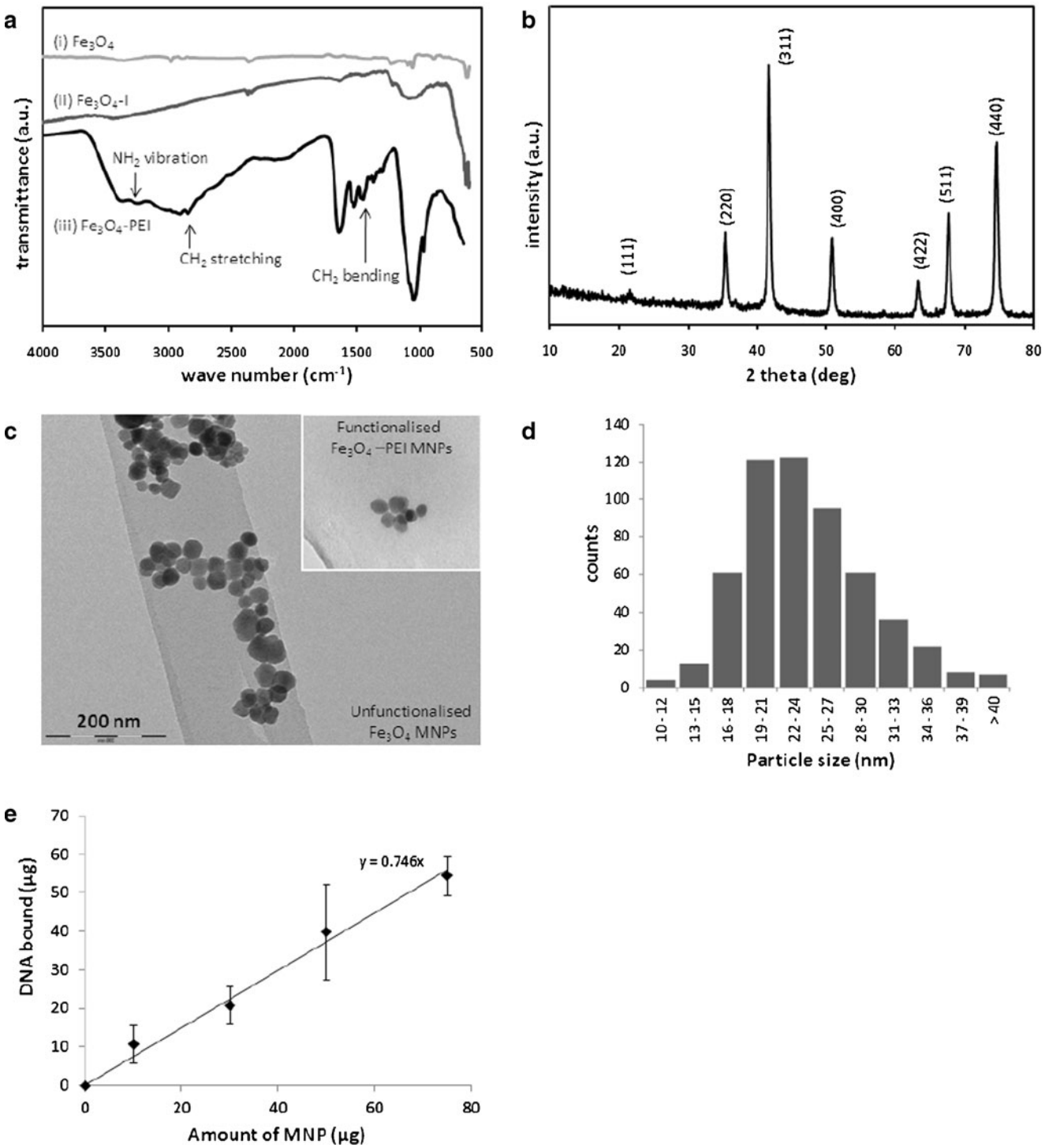

Fig. 2 Characterisation of Fe_3O_4 nanoparticles. (**a**) FTIR spectroscopy of unfunctionalised Fe_3O_4, Fe_3O_4-I (grafted with iodopropyl groups) and Fe_3O_4-PEI. Characteristic bands (NH_2 vibration, CH_2 stretching, and CH_2 bending) for PEI polymer chains are shown. (**b**) XRD diffraction pattern of Fe_3O_4 MNPs (25 nm). This shows a typical inverse spinel structure of Fe_3O_4 (**c**) TEM image of unfunctionalised Fe_3O_4; inset shows a TEM image of Fe_3O_4-PEI MNPs (same magnification as the main figure); (**d**) Particle size distribution (using TEM analysis, $n = 550$); a mean size of 24.3 ± 5.7 nm was determined; (**e**) DNA binding curve for Fe_3O_4-PEI MNPs; the DNA binding capacity (746 μg DNA per mg MNPs) was determined by the slope of the plot.

nanoparticle. These values suggest that the iron content of the Fe_3O_4-PEI-RITC is around 58%, which is far higher than for standard commercial reagents for magnetofection (usually around 5–10%). The morphology of Fe_3O_4-PEI-RITC was studied using TEM and these were found to have a spherical morphology; the morphology was not

found to be affected by the multi-step functionalisation procedure (Fig. 2c). Our TEM analyses demonstrate that the mean core size of these Fe_3O_4-PEI-RITC particles was 24.3±5.7 nm (n=550) (Fig. 2d), which is significantly smaller than the overall particle size of commercial MNPs (usually >150 nm). As observed from the TEM images, many Fe_3O_4-PEI-RITC particles were coated individually and a significant number of such isolated particles were found during the analysis. The measurement of MNP core size from the TEM analysis was also in agreement with the XRD analysis, in which an average crystal size of 25.5 nm was calculated using Scherer analysis. This approach for particle size analysis was preferred to methods such as dynamic light scattering (DLS) as the latter does not represent a robust approach for characterising heavy inorganic particles; sizing using DLS often yields data on hydrodynamic size of the objects in suspensions of MNPs that is larger than the overall size of insulated particles (*i.e.* particles without charge). This is commonly observed for suspensions of MNPs as aggregates can be easily formed due to dipole-dipole interactions. Moreover, DLS is more accurate for soft materials such as polymers or proteins and overestimation in particle size is likely for denser materials (23). By grafting PEI onto the MNP surface, the zeta potential of the particles was found to increase from +10.8 mV to +18.6 mV, suggesting the introduction of positive charges for DNA binding. The DNA binding capacity of the Fe_3O_4-PEI MNPs was measured as 746 μg DNA per mg of particles (Fig. 2e). Table I summarises the key physicochemical properties of the particles and compares these with several PEI coated Fe_3O_4 MNPs synthesised by other methods (21,24–28).

MRI Contrast Property of Fe_3O_4-PEI-RITC MNPs

The MRI properties of the Fe_3O_4-PEI-RITC MNPs were assessed by measuring the transverse relaxation time T_2, on a 7T MRI scanner. Fe_3O_4-PEI-RITC MNPs of iron concentrations between 0.01 and 0.2 mM were measured at room temperature. Their efficiency as contrast agents was determined by calculating the transverse relaxation rate ($R_2 = 1/T_2$) from a linear fit of the inverse relaxation times as a function of the iron concentration. As shown in Fig. 3a, the signal intensity of T_2-weighted images decreased with the increase in Fe concentration. Also, Fig. 3b shows the transverse relaxation rates $1/T_2$ against the different iron concentrations. As expected, the relaxation rates vary with the iron concentration and the relaxivities (equivalent to the slopes of the lines) of Fe_3O_4-PEI-RITC MNPs was found to be 107.3 mM^{-1} s^{-1}, lower than that of unfunctionalised Fe_3O_4 MNPs (147.8 mM^{-1} s^{-1}). However, it is difficult to directly compare these results with those from the literature because the parameters of measurements, such as field strength, would be different. Nonetheless, this measurement suggests that the Fe_3O_4-PEI-RITC MNPs could be employed as potential MRI contrast agents and that the functionalisation does not adversely affect the relaxation characteristics.

Astrocyte Culture Purity and MNP Uptake

A total of three astrocyte cultures were employed in this study. Culture purity was consistently high as judged by assessment of the proportion of GFAP expressing cells (96.5±0.1%). The majority (94.2±0.4%) of $GFAP^+$ cells exhibited a flattened, polygonal appearance characteristic of type 1 astrocytes, whilst cells with more complex, branching morphologies, typical of type 2 astrocytes, accounted for the remaining 5.8% of the total $GFAP^+$ cell population.

MNP Uptake and Retention

Microscopic assessment of live cells following incubation with MNPs, revealed a rapid and extensive accumulation of

Table I Comparison of Physicochemical Properties of Novel Fe_3O_4-RITC-PEI Particles (First Entry) and Selected, Previously Characterised Fe_3O_4-PEI Particles

Particle	Core crystal size (nm)	Magnetization of iron oxide core at 1T (emu/g Fe_3O_4)	Fe content	PEI content	PEI Mw (Da)	Ref
Fe_3O_4-PEI-RITC	24	80	57%	22%	1,800	
Fe_3O_4-PEI	27±12	Not shown	29%	60%	25,000	(24)
Fe_3O_4-PLA-PEI	Not shown	30[a]	8%	17%	10,000	(25)
Fe_3O_4-SiO_2-PEI	10	31	<8%	1.1%, 2.7%	423, 1,800	(21)
Fe_3O_4-PEI	10±2	Not shown	29%	60%	25,000	(26)
Fe_3O_4-PEI	11–25	74	Not shown	Not shown	25,000	(27)
Fe_3O_4-PEI	8, 16, 30	41, 27, 75	Not shown	Not shown	25,000	(28)

[a] estimated from the iron oxide content and measured overall magnetisation of the composite material

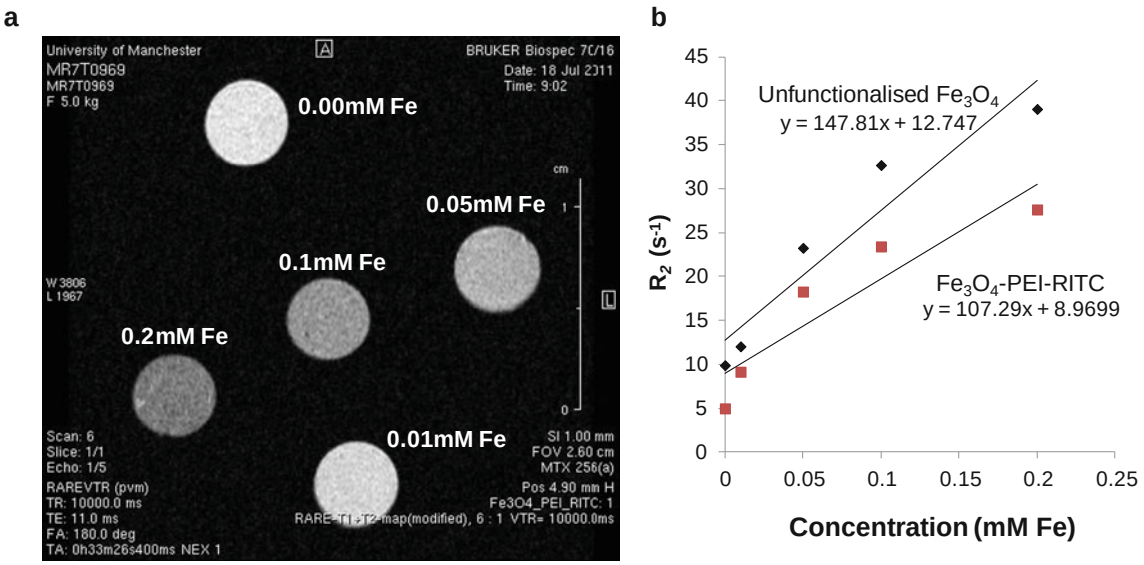

Fig. 3 MRI study on Fe_3O_4-PEI-RITC MNPs. (**a**) Moderately T_2 weighted (TE/TR 11/10 000 ms) MR images of Fe_3O_4-PEI-RITC MNPs and (**b**) R_2 transverse relaxation rate plotted (*red squares*) as function of Fe concentration, compared with unfunctionalised Fe_3O_4 MNPs (*black diamond*).

particles in cells incubated with the highest particle dose studied (67 μg/ml). At 1 h post-addition, >80% cells showed varying degrees of RITC-associated fluorescence (data not shown). By 24 h, near-complete labelling of cells was apparent, with both type 1 and type 2 astrocytes clearly showing MNP uptake (Fig. 4a). Whilst the majority of $GFAP^+$ cells demonstrated particle uptake, cellular heterogeneity was evident in cultures with respect to the extent of particle accumulation. Based on differential particle accumulation, cells could be categorised as demonstrating heavy, medium and light uptake (Fig. 4a). Particles showed a marked tendency to accumulate around the nucleus, *i.e.* perinuclear labelling, and this was more pronounced at 48 h (Fig. 4b) than at 24 h (Fig. 4a) *post*-particle application. Phase contrast microscopy revealed characteristic brownish intracellular deposits of particles, both in the perinuclear regions as well as in the cytosol (Fig. 4b, inset). Long term monitoring of cells in pulse-labelling experiments, revealed that the majority (*ca* 74%) of cells which had been incubated with 67 μg/ml Fe_3O_4-PEI-RITC showed some degree of particle retention for up to 6 days, although the distinctive pattern of perinuclear localisation of particles was no longer apparent for labelled cells at this time point (Fig. 4c).

Perl's histochemical stain confirmed the presence of iron in cells post-particle application (Fig. 4d). In all experiments, a negative Perl's stain was obtained for control cells incubated in the absence of particles. Heterogeneity in cellular accumulation of particles was also apparent following Perl's staining (Fig. 4d), confirming findings obtained by direct observation of RITC labelling in astrocytes by fluorescence microscopy (Fig. 4a). This histochemical method was effective at detecting even small intracellular particle accumulations (Fig. 4d).

Quantitative determination of cellular MNP uptake, revealed clear-cut concentration dependence at 24 h with and without particle complexation to DNA (Fig. 4e). No differences in the extent of uptake were observed between incubations containing particles alone or particles complexed with DNA at any particle concentration (Fig. 4e). In both cases, a particle concentration of 67 μg/ml was sufficient to achieve labelling of virtually all cells (96.6±0.7% for particles alone; 97.7±0.3% for particles complexed with DNA).

Transfection Mediated by Fe_3O_4-RITC-PEI Particles

In order to examine the gene delivery potential of the particles, complexes were formed with a plasmid encoding the reporter protein, GFP, prior to adding to cells; a range of particle concentrations were studied at constant particle: DNA ratios. In line with several previous studies in neural transplant cells, no transfection was ever observed using plasmids alone (7,8,18). At the highest particle concentration (67 μg/ml), transfected astrocytes of type 1 and type 2 morphology were seen at 48 h after complex addition (Fig. 5a), including type 1 cells which appeared to have recently undergone cell division (Fig. 5b). However, transfection efficiencies were consistently low (<1%; $n=3$ cultures). We deemed it unnecessary to apply free PEI with $M_w=1{,}800$ to cell cultures, as there is extensive evidence from the literature to show that this molecular weight PEI alone does not yield transfection (29). Regular

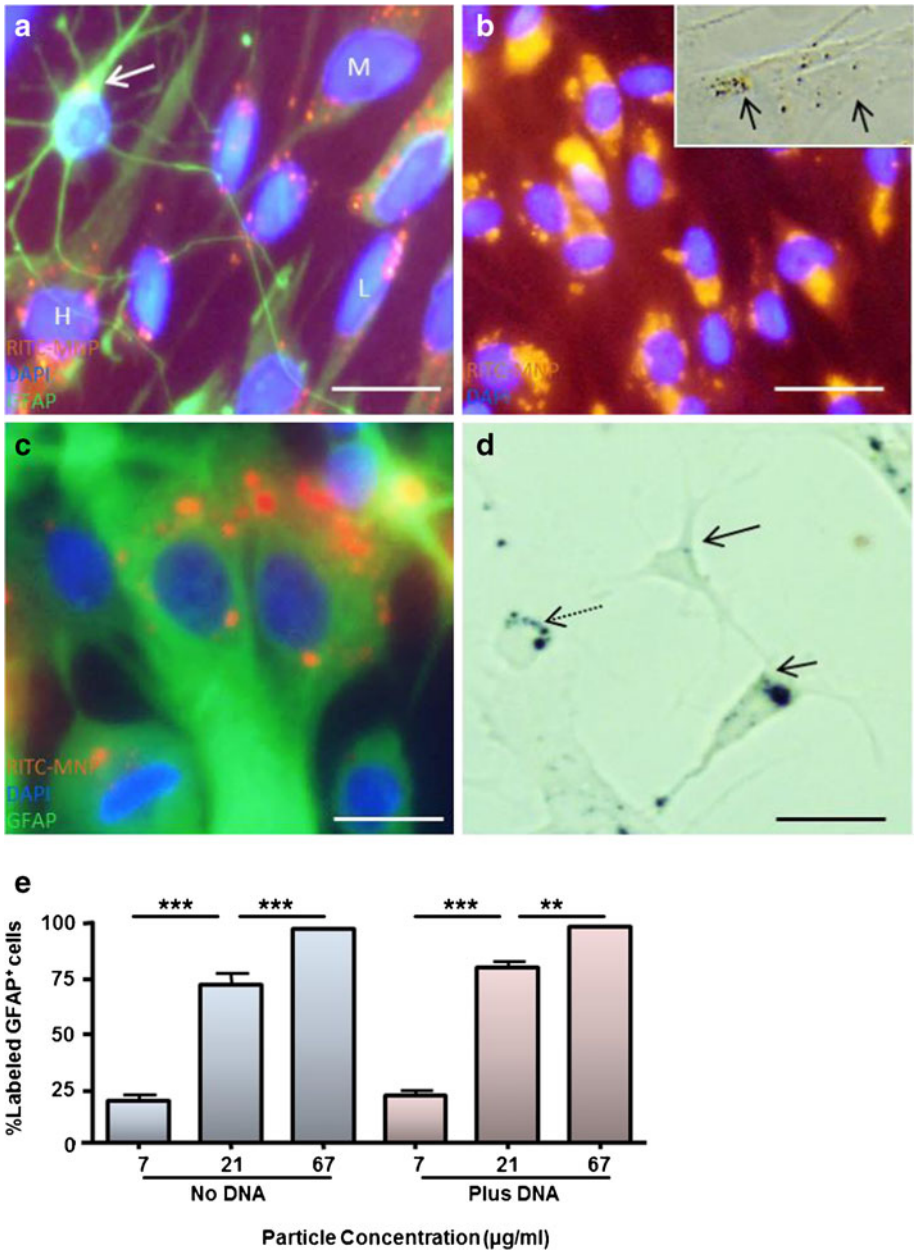

Fig. 4 Particle uptake by astrocytes. (**a**) Representative triple-merged image showing particle uptake in astrocyte cultures at 24 h after addition of particles (67 μg/ml). Note that some type 1 astrocytes (labelled 'L') exhibit low levels of particle accumulation, whereas others exhibit moderate (labelled 'M') and high (labelled 'H') levels of particle accumulation. The *arrow* indicates a type 2 astrocyte, which also exhibits particle uptake. (**b**) Representative double-merged image showing particle localisation in the perinuclear region of most cells at 48 h after addition of particles (67 μg/ml). The inset show a high magnification phase contrast view of two unstained astrocytes (*arrows*) with characteristic brownish intracellular clusters of MNPs. (**c**) Representative triple-merged image of astrocytes at 144 h after incubation with particles (67 μg/ml) for 4 h. Note that the majority of cells still exhibit particle retention, but in some cells particles are no longer associated with the perinuclear region. (**d**) Representative image of astrocytes which have been reacted with Perl's stain at 24 h after incubation with particles (67 μg/ml). Note that cells with low (*long arrow*) and high (*short arrow*) levels of iron accumulation are evident, with some cells (*dashed arrow*) demonstrating a clear perinuclear localisation of iron deposits. (**e**) *Bar chart* showing the concentration-dependence of cell labelling efficiency in 24 h incubations with particles alone ('no DNA') or particles complexed with DNA ('plus DNA'). In each case, labelling efficiency is clearly dependent on particle concentration $^{**}p < 0.01$ and $^{***}p < 0.001$ *versus* the preceding particle concentration; $n = 3$ cultures; one-way ANOVA and Bonferroni's *post*-tests. Note that there was no difference between particles alone or particles complexed with DNA at any particle concentration. Scale bars are 25 μm in (**a**), 50 μm in (**b**, **d**) and 10 μm in (**c**).

observation of live cultures by combined phase and fluorescence microscopy for up to 96 h *post*-complex addition revealed that the onset of GFP expression was at approximately 42 h and expression plateaued at 48 h. In samples which had been fixed at 48 h and observed without immunostaining for GFAP, relatively large

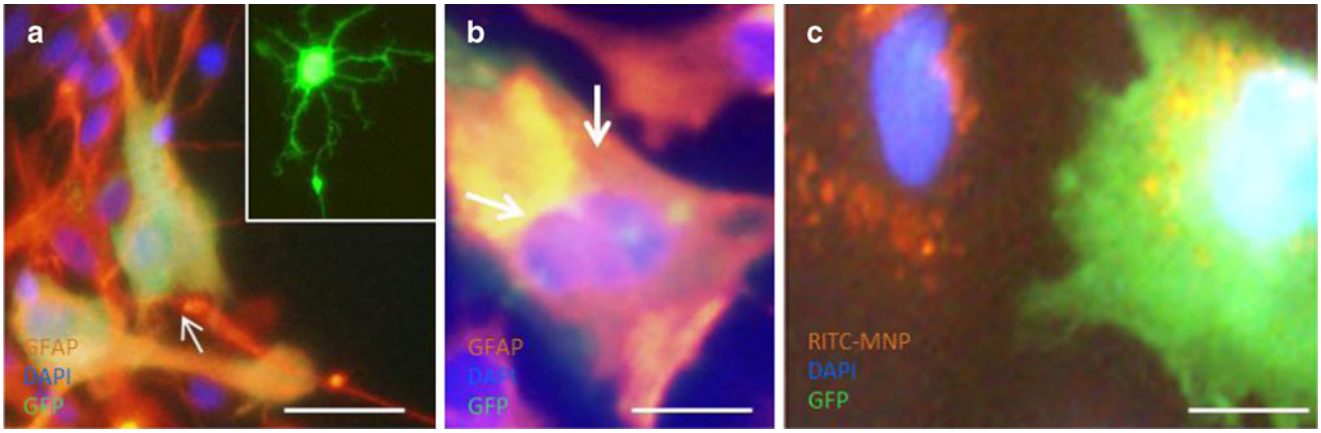

Fig. 5 Particle-mediated transfection in astrocytes. (**a**) Representative triple-merged image showing GFP expression by two neighbouring $GFAP^+$ astrocytes of type 1 morphology indicated by *arrow*, at 48 h after adding particle/DNA complexes; inset is a unmerged image showing GFP expression in a cell which morphologically resembles a type 2 astrocyte. (**b**) Representative triple-merged image showing GFP expression in two $GFAP^+$ astrocytes (indicated by *arrows*) which appear to have arisen from a recent cell division. (**c**) Representative triple-merged image showing co-localisation of GFP expression and Fe_3O_4-PEI-RITC particles in a cell of type 1 astrocyte morphology. Note that the neighbouring GFP^- cell exhibits a similar level and subcellular distribution of particles without transfection. Scale bars are 50 μm in (**a**), 20 μm in (**b**) and 10 μm in (**c**).

accumulations of particles with a predominantly perinuclear localisation could be seen not only in GFP-expressing cells, but also in adjacent non-transfected cells (Fig. 5c).

Magnetofection Experiments

Commercial, transfection-grade MNPs, such as Neuromag, can successfully mediate gene delivery to astrocyte cultures; basal transfection efficiencies of approximately 10% have been reported, and these can be enhanced (three-fold) by the application of a static magnetic field (18). Indeed, in quality control experiments using the same cultures of astrocytes and the same batch of pmaxGFP employed here, effective gene delivery by Neuromag was observed, and this was enhanced by the application of a static magnetic field, in line with our previously published results (18). With respect to Fe_3O_4-PEI-RITC particles, application of a static magnetic field had no effect on transfection efficiency, which remained low (<1%). To exclude any adverse effect of the RITC tag on gene delivery, magnetofection experiments were repeated with Fe_3O_4-PEI particles (*i.e.* lacking the RITC tag), but these also yielded low transfection efficiency (<1% ± static magnetic field) similar to Fe_3O_4-PEI-RITC particles.

MNP Toxicity

At all time points and with all particle concentrations studied here, particle-treated cells appeared healthy as judged by a number of parameters, including the morphological appearance of cells, their proliferative potential and the intensity/pattern of cellular GFAP immunostaining (Fig. 6a and b). Quantitation of cell density at 24 h revealed that this remained similar between control and particle-treated cultures, irrespective of whether particles alone or particle/DNA complexes were added to cultures (Fig. 6c), indicating no adverse effects of particles on cell adherence. The proportions of $GFAP^+$ cells (Fig. 6d) and type 1/type 2 astrocytes (data not shown) also remained unaffected by particle treatment. Finally, the proportions of pyknotic cells in astrocyte cultures, as judged from the morphological assessment of DAPI-stained nuclei, remained low with and without particle addition, indicating limited occurrence of cell death (Fig. 6e). Further, in longer term experiments, labelled cultures reached confluency, similar to controls, indicating no adverse effects of the particles on the proliferative capacity of astrocytes.

DISCUSSION

We describe a novel coating methodology for covalently grafting PEI onto the surface of Fe_3O_4 MNPs without a non-functional polymer layer. Most PEI grafted MNPs reported in the literature to date, have been based on PEI bound onto a thick, primary coating such as dextran or synthetic polymers (24–26). Our chemical approach offers four important advantages over other coating strategies described so far, to synthesise PEI coated MNPs for use in biological systems. First, the PEI molecules are covalently linked to the MNP core, via a monolayer of –Si–O– coating from the silane grafting process during the first step. The resultant PEI coating is permanent in contrast to methods that involve PEI coating onto the MNP surface via electrostatic interactions. When the latter are dispersed

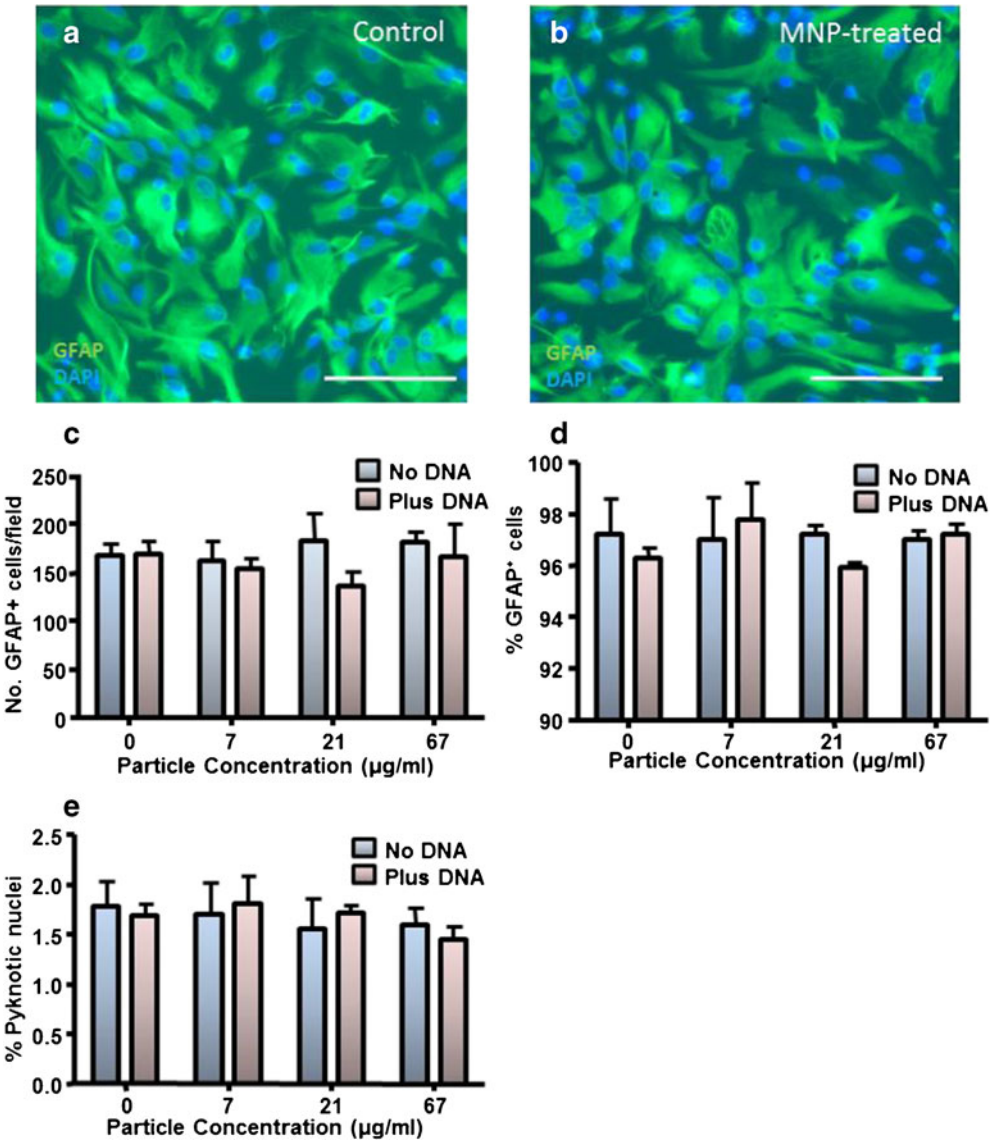

Fig. 6 Quantitative analysis of particle toxicity in astrocytes. (**a**) Representative double-merged image showing control astrocyte cultures or (**b**) after particle (67 μg/ml) addition, at 24 h. Note that cell density, cell morphology and pattern of immunostaining is similar to that in (**a**). (**c**–**e**) *Bar charts* showing densities of $GFAP^+$ cells (**c**) the proportions of $GFAP^+$ cells (**d**) and the proportions of cells with pyknotic nuclei (**e**), at 24 h after addition of the indicated concentrations of particles alone ('no DNA') or particles complexed with DNA ('plus DNA'). Values for all parameters were similar to controls for cultures treated with particles alone or particles complexed with DNA, irrespective of the particle concentration ($n = 3$ cultures; one-way ANOVA and Dunnett's MCT). Scale bars in (**a**) and (**b**) are 100 μm.

in solutions containing high electrolyte concentrations (for example, biological fluids *in vivo*), passively coated PEI molecules are likely to detach from the MNP cores due to the competition from other positively charged species such as Na^+. Second, compared with PEI grafted onto crosslinked polymer coated MNPs, *e.g.* dextran-MNPs or chitosan-MNPs, our design minimises the use of such non-functional layers. This is important as with crosslinked polymer coatings, it is difficult to restrict overall particle size to <150 nm as these particles form large clusters of small MNPs (from 5 to 25 nm) during the crosslinking process; decreased particle size in turn may increase cellular uptake and enhance cellular safety. Third, use of non-functional polymers reduces the overall iron content of the MNPs; from an MR imaging perspective, high iron content is preferred as a higher contrast can be generated, providing that the crystallinity of the iron oxide core remains the same. Our chemical design allows direct functionalisation of the surface of the MNPs by "cutting out the middle-man" (*i.e.* the non-functional polymers). Finally, crosslinked polysaccharide coated MNPs are likely to degrade as these polymer chains are vulnerable to enzymatic degradation resulting in potential release of Fe_3O_4 MNPs from the composite particle and rendering such particles unsuitable for successful long-term tracking of cells. Our design avoids the use of bio-degradable components and enzymatic degradation is therefore avoided.

We have demonstrated proof of the MNP-polymer grafting concept using PEI (as an example of a widely used functional transfection grade polymer) but this design can be applied more widely to the grafting of other functional polymers, such as polylysine. It should be noted that many other alkoxysilanes with various organic functional groups

are available commercially, with alternative binding chemistries including amide coupling and click chemistry that can also be used for particle functionalisation using our approach, indicating the versatility of the method. Rhodamine B fluorescent dye, commonly used for cell labelling applications (30), was tagged onto the amine groups of PEI skeleton. This is unlikely to affect the positively charged nature of the PEI; other workers have reported that RITC binding efficiency onto a polymer (chitosan) is only 2.0% (31), suggesting that most of the amine groups are preserved following fluorophore tagging. Hence, the DNA binding capacity of the particles is unlikely to be affected. This protocol is not limited to RITC, since many fluorophores that are commonly used currently to tag biomolecules, were designed to target the lysine groups (-NH_2 groups) of a protein molecule; examples include the isothiocyanate- (ITC) and the succinimidyl ester-derivatives of common dyes, such as the Alexa Fluor family. Further functionalisation on the PEI skeleton for tagging other functional entities is also possible. For example, the primary amine groups on the PEI skeleton can also be used to bind protein/peptides via a glutaraldehyde linker (32), allowing for further targeting of the MNPs to particular neural cell types or intracellular compartments.

Compared with many commercial MRI contrast reagents, the enhanced iron content of these Fe_3O_4-PEI-RITC MNPs represents a possibility for higher MRI contrast capability. However, there is an upper limit to the iron content of iron oxide based MNPs as uncoated magnetite (Fe_3O_4) has an iron content of 72.4%. This value means that even if the coating materials are limited to about 10% by weight, an iron content of about 65% is the realistic maximum. For long term monitoring, the degradation profile of the MNP iron core is an issue of paramount significance. Rapid degradation of the iron oxide core after internalisation would result in the loss of MRI contrast signal with subsequent difficulties in reliable monitoring of transplant populations. In our ongoing experiments using ultrastructural analyses of intracellular MNP localisation and morphology, 25 nm MNPs, coated with polyvinyl alcohol (PVA) and tagged with FITC, were found to be present in high numbers within mouse embryonic stem cells even after 7 days post-labelling, without overt signs of particle degradation or iron leaching (33), suggesting that the Fe_3O_4-RITC-PEI particles can also be adapted for longer term tracking of transplanted cell populations.

The multimodal Fe_3O_4-PEI-RITC MNP synthesised using a chemical grafting approach, is compatible for safe use with astrocytes and can mediate cell labelling and imaging, with limited ability for gene delivery. This 'prototype' MNP therefore has considerable potential, after further development, to function as a 'multifunctional platform' for neural cell transplantation therapies. This is of importance, given the critical lack of available nanoplatforms that can mediate both therapeutic and imaging modalities in neural cells. Regarding the culture model used for these analyses, it should be noted that cell lines (of both neural and non-neural origin) have been widely used in previous studies to evaluate MNP applications. These frequently exhibit genetic instability and abnormal cell behaviour secondary to cell transformation. For example, compared with untransformed cells, cell lines often exhibit resistance to cell death stimuli (of relevance when determining the safety of MNP-based procedures), as well as abnormally high transfection efficiencies with non-viral transfection agents (of relevance when assessing the gene delivery potential of MNPs). The present study has used astrocytes derived from primary cultures, in order to rigorously evaluate the properties of the prototype multimodal MNPs within a culture system that avoids the above drawbacks associated with cell lines.

In terms of particle safety for biological applications, compared with other silane-based grafting routes *via* the use of APTES (32), our particle coating has avoided the use of non-functional spacers, such as glutaraldehyde, which can be weak points in the coating due to the possible hydrolysis of imine and may introduce unwanted toxicity to the resultant materials (34), whereas the synthesised particles were not associated with cytotoxic effects in astrocytes, at the concentrations studied here. The MNPs could be detected in the majority of astrocytes by 1 h post-incubation, whereas longer incubations (*ca* 4 h) were required in a previous study to achieve the same extent of cellular labelling with similar concentrations of 360 nm MNPs (17). This suggests that the rate of particle accumulation is faster in the case of these smaller particles; particles in the sub-50 nm range are known to be taken up via clathrin and caveolin mediated mechanisms in a wide range of cell types (uptake mechanisms that are known to occur more rapidly than macropinocytosis) (35). Indeed, our experiments to achieve cell labelling and gene delivery employing these novel particles used technically uncomplicated experimental procedures, involving simple incubation of cells with particles alone or with particle-plasmid complexes and it was possible to rapidly achieve labelling of >96% of astrocytes whilst using particle concentrations that exhibited negligible toxicity.

Our findings also demonstrate that the particles offer compatibility with fluorescence and light microscopy (in combination with histochemical methods) to study nanoparticle uptake and trafficking. The high iron content of particles should also make these amenable to high resolution, ultrastructural TEM analyses to

study intracellular particle processing and fate, as previously demonstrated by ourselves in astrocytes for larger particles with lower iron content (20% w/v Fe) (17). This versatility for use with a diverse range of histological methods will facilitate a comprehensive and detailed characterisation of the intracellular handling of particles, along with long term particle retention and safety in host tissue. These parameters are critical to establish for neural transplant cells in particular, where cell safety and phenotypic stability are key considerations for the long term survival and integration of grafts.

The above features of the particles offer a number of key advantages in transplantation neurobiology, in terms of the technical simplification of experiments and reduced manipulation of cells prior to transplantation, of relevance from a health and safety perspective when considering the clinical translation of experimental therapies. Further, the ability to simultaneously achieve cell labelling, cell imaging and gene delivery to cells using a single multifunctional particle in a safe, 'one-step' procedure (within the same experiment), would be of considerable benefit to the standardisation, development and evaluation of cell therapies. Such an approach can reduce the need to conduct multiple (parallel) experiments, each employing different technical procedures for transfection, cell targeting, non-invasive imaging and histological analyses of cells *post*-transplantation. By extrapolation, a unified approach facilitated by development of multimodal MNPs such as that proposed here, will help reduce experimental animal usage whilst accelerating the rate of development of transplantation strategies for neural repair. This is a desirable goal from both the ethical and economic viewpoints.

Although the Fe_3O_4-PEI-RITC MNPs demonstrated transfection capability, the efficiency of gene transfer is low (<1%). This is significantly lower than that achievable using commercial reagents, which produce basal transfection efficiencies of up to 10% in astrocytes, even in the absence of a magnetic field (18). This low transfection is observed despite rapid and extensive particle uptake after complex formation and the subsequent accumulation of particles in the perinuclear region (a pre-requisite for plasmid delivery to the nucleus). It is not clear currently, what mechanisms underlie the low transfection efficiency. First, quality control experiments using commercial transfection grade particles (*i.e.* Neuromag) resulted in expected levels of GFP expression, ruling out problems with the pmaxGFP plasmid or the transfection competence of the cells as causal factors. Second, use of Fe_3O_4-PEI nanoparticles (*i.e.* without the RITC tag) produced low transfection efficiencies, similar to findings with Fe_3O_4-PEI-RITC MNPs. This rules out adverse effects of RITC conjugation to PEI moieties on gene delivery rates. However, other factors may account for the low transfection efficiency, including the kinetics of DNA binding/release by particles. For example, with commercial transfection-grade MNPs, the onset of GFP expression in astrocytes is rapid (within 4 h) whereas, with Fe_3O_4-PEI-RITC MNPs, GFP expression was never seen before 42 h. This is indicative of slow rates of DNA dissociation from particles, which may be related to the PEI chain length or altered conformation of PEI moieties secondary to the strong, permanent bonding between the PEI and the MNP surface. A recent study on Fe_3O_4-PEI MNPs has shown that short chain PEI covalent coating has a high affinity to DNA molecules with a low N/P ratio (nitrogen to phosphorous, a ratio for measuring the binding efficiency per amine group) (36). The reduced release of bound GFP plasmid from the Fe_3O_4-PEI-RITC may result in low transfection rates. Further work on the DNA release kinetics of the prototype particles and their modes of intracellular trafficking is essential to optimise their gene delivery potential. Changes in PEI chain length, the method of PEI grafting to the Fe_3O_4 core, or the use of DNA binding agents other than PEI, may improve plasmid dissociation from particles (and hence transfection) should the problem lie with suboptimal DNA binding/release properties of the particles. Alternatively, if the route of cellular particle trafficking is identified as the underlying basis for the low transfection efficiency of particles, then this will require modifications in particle design, for example, to target particles to a pro-transfection route of uptake (17).

The efficiency of magnetofection techniques (use of applied magnetic fields to assist transfection) (37) has been demonstrated previously for astrocytes using Neuromag particles (18). It is not currently clear what accounts for the absence of effects of magnetofection strategies on gene transfer mediated by the Fe_3O_4-RITC-PEI particles. Application of static magnetic fields is thought to sediment particles over cells, increasing the local concentration of transfection complexes at the cell surface, thereby overcoming the first barrier to transfection, namely particle access to cells (38). We have observed rapid accumulation of the Fe_3O_4-RITC-PEI particles in cells without field application; additionally, receptor-mediated endocytotic mechanisms characteristically display saturation kinetics. Such saturating levels in the absence of a magnetic field imply that magnetofection would have no additional beneficial effect on uptake and hence gene delivery. Alternative explanations cannot be ruled out, however. For example, due their high iron content, Fe_3O_4-RITC-PEI MNPs are likely to form compact aggregates after magnetization which may further hinder the release of GFP plasmid, potentially addressable by systematically varying the Fe content, colloidal stability or size of the particles to achieve compatibility with magnetofection methods. Additionally, the effects of novel magnetofection methods employing oscillating magnetic fields (8), on these small diameter, high Fe content particles also remain to be established.

CONCLUSIONS

A fluorescent MNP with high iron content and limited transfection capability can be assembled by grafting PEI onto the MNP surface via a silanisation process, followed by RITC binding onto the PEI polymer. This multi-step synthetic pathway opens up a new avenue for the multifunctional surface design of MNPs for biological applications. Although not demonstrated here, incorporation of other functionalities can be made possible by tagging further functional groups onto the PEI branches. As such, designs of greater functional complexity can be evolved from this basic particle model. Such particles are well tolerated by astrocytes, a major neural cell transplant population, with no signs of cytotoxicity and could be used for cell labelling and imaging applications. After further refinements directed towards the enhancement of their gene delivery properties, the Fe_3O_4-RITC-PEI particles described here are likely to prove a valuable 'theragnostic' tool for the development and clinical translation of neural cell therapies.

A major challenge in developing multifunctional MNPs is the constraint in availability of space on the MNP surface to accommodate a number of functional entities. This is generally achieved by the use of long chain functional polymers that can be associated with an increase in the overall size of the particles. Making use of short polymers and their functional groups for tethering functional entities, such as a fluorescent tag, can offer a viable solution as we demonstrate here, provided that interference, such as steric hindrance and non-specific conjugations, between these entities is minimised.

ACKNOWLEDGMENTS & DISCLOSURES

DMC is supported by a New Investigator Award from the British Biotechnology and Biological Sciences Research Council. The authors acknowledge EPSRC (EP/C511794) for financial support. We thank Dr. James Long (IOTA Nanosolutions) for the zeta potential measurements and Dr. Laurent Bouffier (now at Université Bordeaux) for his assistance with FTIR spectroscopy and Ms Karen Davies who performed the MRI measurements at the University of Manchester.

REFERENCES

1. Gögel S, Gubernator M, Minger SL. Progress and prospects: stem cells and neurological diseases. Gene Ther. 2011;18(1):1–6.
2. Chari DM. Remyelination in multiple sclerosis. Int Rev Neurobiol. 2007;79:589–620.
3. Herranz F, Almarza E, Rodríguez I, Salinas B, Rosell Y, Desco M, Bulte JW, Ruiz-Cabello J. The application of nanoparticles in gene therapy and magnetic resonance imaging. Microsc Res Tech. 2011;74(7):577–91.
4. Gleave JA, Valliant JF, Doering LC. ^{99m}Tc-based imaging of transplanted neural stem cells and progenitor cells. J Nucl Med Tech. 2011;39(2):114–20.
5. Chari DM, Blakemore WF. New insights into remyelination failure in multiple sclerosis: implications for glial cell transplantation. Mult Scler. 2002;8(4):271–7.
6. Ruff CA, Wilcox JT, Fehlings MG. Cell-based transplantation strategies to promote plasticity following spinal cord injury. Exp Neurol. 2011. doi:10.1016/j.expneurol.2011.02.010.
7. Pickard MR, Barraud P, Chari DM. The transfection of multipotent neural precursor/stem cell transplant populations with magnetic nanoparticles. Biomaterials. 2010;32(9):2274–84.
8. Jenkins SI, Pickard MR, Granger N, Chari DM. Magnetic nanoparticle-mediated gene transfer to oligodendrocyte precursor cell transplant populations is enhanced by magnetofection strategies. ACS Nano. 2011;5(8):6527–38.
9. McBain SC, Yiu HHP, Dobson J. Magnetic nanoparticles for gene and drug delivery. Int J Nanomed. 2008;3(2):169–80.
10. Hyeon T. Chemical synthesis of magnetic nanoparticles. Chem Commun. 2003;8:927–34.
11. Berry CC, Curtis ASG. Functionalisation of magnetic nanoparticles for applications in biomedicine. J Phys D Appl Phys. 2003;36(13):R198–206.
12. Yiu HHP, McBain SC, Lethbridge ZAD, Lees MR, Dobson J. Preparation and characterization of polyethylenimine-coated Fe_3O_4-MCM-48 nanocomposite particles as a novel agent for magnet-assisted transfection. J Biomed Mater Res A. 2010;92A (1):386–92.
13. Veiseh O, Sun C, Fang C, Bhattarai N, Gunn J, Kievit F, Du K, Pullar B, Lee D, Ellenbogen RG, Olson J, Zhang MQ. Specific targeting of brain tumors with an optical/magnetic resonance imaging nanoprobe across the blood-brain barrier. Cancer Res. 2009;69(15):6200–7.
14. Olariu CI, Yiu HHP, Bouffier L, Nedjadi T, Costello E, Williams SR, Halloran CM, Rosseinsky MJ. Multifunctional Fe_3O_4 nanoparticles for targeted bi-modal imaging of pancreatic cancer. J Mater Chem. 2011;21(34):12650–9.
15. Lu AH, Salabas EL, Schuth F. Magnetic nanoparticles: synthesis, protection, functionalization, and application. Angew Chem Intl Ed. 2007;46(8):1222–44.
16. Berman SMC, Walczak P, Bulte JWM. Tracking stem cells using magnetic nanoparticles. Wiley Interdiscip Rev Nanomed Nanobiotechnol. 2011;3(4):343–55.
17. Pickard MR, Jenkins SI, Koller CJ, Furness DN, Chari DM. Magnetic nanoparticle labeling of astrocytes derived for neural transplantation. Tissue Eng C Meth. 2011;17(1):89–99.
18. Pickard M, Chari D. Enhancement of magnetic nanoparticle-mediated gene transfer to astrocytes by 'magnetofection': effects of static and oscillating fields. Nanomedicine. 2010;5(2):217–32.
19. Nishida K, Tanaka N, Nakanishi K, Kamei N, Hamasaki T, Yanada S, Mochizuki Y, Ochi M. Magnetic targeting of bone marrow stromal cells into spinal cord: through cerebrospinal fluid. Neuroreport. 2006;17(12):1269–72.
20. Veiseh O, Kievit FM, Fang C, Mu N, Jana S, Leung MC, Mok H, Ellenbogen RG, Park JO, Zhang MQ. Chlorotoxin bound magnetic nanovector tailored for cancer cell targeting, imaging, and siRNA delivery. Biomaterials. 2010;31(31):8032–42.
21. McBain SC, Yiu HHP, El Haj A, Dobson J. Polyethyleneimine functionalized iron oxide nanoparticles as agents for DNA delivery and transfection. J Mater Chem. 2007;17(24):2561–5.
22. Hennig J, Nauerth A, Friedburg H. RARE imaging: a fast imaging method for clinical MR. Magn Reson Med. 1986;3 (6):823–33.

23. Hall JB, Dobrovolskaia MA, Patri AK, McNeil SE. Characterization of nanoparticles for therapeutics. Nanomedicine. 2007;2(6):789–803.
24. Steitz B, Hofmann H, Kamau SW, Hassa PO, Hottiger MO, von Rechenberg B, Hofmann-Amtenbrink M, Petri-Fink A. Characterization of PEI-coated superparamagnetic iron oxide nanoparticles for transfection: size distribution, colloidal properties and DNA interaction. J Magn Magn Mater. 2007;311(1):300–5.
25. Chorny M, Polyak B, Alferiev IS, Walsh K, Friedman G, Levy RJ. Magnetically driven plasmid DNA delivery with biodegradable polymeric nanoparticles. FASEB J. 2007;21(10):2510–9.
26. Petri-Finka A, Steitza B, Finka A, Salaklanga J, Hofmann H. Effect of cell media on polymer coated superparamagnetic iron oxide nanoparticles (SPIONs): colloidal stability, cytotoxicity, and cellular uptake studies. Eur J Pharm Biopharm. 2008;68(1):129–37.
27. Arsianti M, Lim M, Marquis CP, Amal R. Assembly of polyethylenimine-based magnetic iron oxide vectors: insights into gene delivery. Langmuir. 2010;26(10):7314–26.
28. Ang D, Nguyen QV, Kayal S, Preiser PR, Rawat RS, Ramanujan RV. Insights into the mechanism of magnetic particle assisted gene delivery. Acta Biomaterialia. 2011;7(3):1319–26.
29. Godbey WT, Wu KK, Mikos AG. Size matters: molecular weight affects the efficiency of poly(ethylenimine) as a gene delivery vehicle. J Biomed Mater Res. 1999;45(3):268–75.
30. Kobbert C, Apps R, Bechmann I, Lanciego JL, Mey J, Thanos S. Current concepts in neuroanatomical tracing. Prog Neurobiol. 2000;62(4):327–51.
31. Ma O, Lavertu M, Sun J, Nguyen S, Buschmann MD, Winnik FM, Hoemann CD. Precise derivatization of structurally distinct chitosans with rhodamine B isothiocyanate. Carbohydr Polym. 2008;72(4):616–24.
32. Can K, Ozmen M, Ersoz M. Immobilization of albumin on aminosilane modified superparamagnetic magnetite nanoparticles and its characterization. Colloid Surf B Biointerfaces. 2009;71(1):154–9.
33. Murray P, Palona I, Yiu HHP, Olariu CI, Rosseinsky MJ. Unpublished results.
34. Lerones C, Mariscal A, Carnero M, Garcia-Rodriguez A, Fernandez-Crehuet J. Assessing the residual antibacterial activity of clinical materials disinfected with glutaraldehyde, o-phthalaldehyde, hydrogen peroxide or 2-bromo-2-nitro-1,3-propanediol by means of a bacterial toxicity assay. Clin Microbiol Infect. 2004;10(11):984–9.
35. Pattnaik G, Rama Raju KS, Heeralal B, Ali S. Nanovehicles: an efficient carrier for active molecules for entry into the cell. Int J Pharm Sci Rev Res. 2010;4(3):3.
36. Yiu HHP, Bouffier L, Boldrin P, Long J, Claridge JB, Rosseinsky MJ. Direct grafting of amine groups onto iron(II, III) oxide nanoparticles to generate a positively charged three-dimensional coating–I: DNA binding through electrostatic interaction. submitted.
37. Scherer F, Anton M, Schillinger U, Henkel J, Bergemann C, Kruger A, Gansbacher B, Plank C. Magnetofection: enhancing and targeting gene delivery by magnetic force *in vitro* and *in vivo*. Gene Ther. 2002;9(2):102–9.
38. Sapet C, Laurent N, Le Gourrierec L, Augier S, Zelphati O. *In vitro* and *in vivo* magnetofection (TM): a move towards gene therapy. Ann Biol Clin. 2010;68(2):133–42.